Distinguishing the Roles of Thylakoid Respiratory Terminal Oxidases in the Cyanobacterium *Synechocystis* sp. PCC 6803[1][OPEN]

Maria Ermakova[2], Tuomas Huokko[2], Pierre Richaud, Luca Bersanini, Christopher J. Howe, David J. Lea-Smith, Gilles Peltier, and Yagut Allahverdiyeva*

Laboratory of Molecular Plant Biology, Department of Biochemistry, University of Turku, Turku FI–20014, Finland (M.E., T.H., L.B., Y.A.); Commissariat à l'Energie Atomique et aux Energies Alternatives, Institut de Biologie Environnementale et de Biotechnologie, Laboratoire de Bioénergétique et Biotechnologie des Bactéries et Microalgues, Cadarache, F–13108 Saint-Paul-lez-Durance, France (P.R., G.P.); Centre National de la Recherche Scientifique, Biologie Végétale et Microbiologie Environnementales, Unité Mixte de Recherche 7265, F–13108 Saint-Paul-lez-Durance, France (P.R., G.P.); Aix Marseille Université, Biologie Végétale et Microbiologie Environnementales, Unité Mixte de Recherche 7265, F–13284 Marseille, France (P.R., G.P.); and Department of Biochemistry, University of Cambridge, Cambridge, CB2 1QW United Kingdom (C.J.H., D.J.L.-S.)

ORCID ID: 0000-0002-9262-1757 (Y.A.).

Various oxygen-utilizing electron sinks, including the soluble flavodiiron proteins (Flv1/3), and the membrane-localized respiratory terminal oxidases (RTOs), cytochrome *c* oxidase (Cox) and cytochrome bd quinol oxidase (Cyd), are present in the photosynthetic electron transfer chain of *Synechocystis* sp. PCC 6803. However, the role of individual RTOs and their relative importance compared with other electron sinks are poorly understood, particularly under light. Via membrane inlet mass spectrometry gas exchange, chlorophyll *a* fluorescence, P700 analysis, and inhibitor treatment of the wild type and various mutants deficient in RTOs, Flv1/3, and photosystem I, we investigated the contribution of these complexes to the alleviation of excess electrons in the photosynthetic chain. To our knowledge, for the first time, we demonstrated the activity of Cyd in oxygen uptake under light, although it was detected only upon inhibition of electron transfer at the cytochrome b_6f site and in Δ*flv1/3* under fluctuating light conditions, where linear electron transfer was drastically inhibited due to impaired photosystem I activity. Cox is mostly responsible for dark respiration and competes with P700 for electrons under high light. Only the Δ*cox/cyd* double mutant, but not single mutants, demonstrated a highly reduced plastoquinone pool in darkness and impaired gross oxygen evolution under light, indicating that thylakoid-based RTOs are able to compensate partially for each other. Thus, both electron sinks contribute to the alleviation of excess electrons under illumination: RTOs continue to function under light, operating on slower time ranges and on a limited scale, whereas Flv1/3 responds rapidly as a light-induced component and has greater capacity.

Cyanobacteria (oxygenic photosynthetic bacteria) inhabit a range of highly variable aquatic and terrestrial environments, which are diverse in light and in the availability of nutrients. With the exception of *Gloeobacter* spp., all cyanobacteria contain a series of internal thylakoid membranes, where a photosynthetic electron transport chain is localized. This electron transport chain consists of four major protein complexes: PSII, cytochrome b_6f (Cyt b_6f), PSI, and ATP synthase, similar to that of eukaryotic photosynthetic organisms (Fig. 1). The photosynthetic electron transfer chain provides energy (ATP) and reducing equivalents (reduced ferredoxin and NADPH) for carbon anabolism and other vital processes.

Following the absorption of photons by the large external light-harvesting antenna, the phycobilisome, the excitation energy is directed to the reaction centers of PSII and PSI, where charge separation occurs. In PSII, this process is followed by splitting of water to molecular oxygen and protons, which are released into the

[1] This work was supported by the Academy of Finland's Centre of Excellence program in Molecular Biology of Primary Producers (2014–2019; grant no. 271832.), the Kone Foundation (to Y.A.), the Alfred Kordelin Foundation (to L.B.), the Environmental Services Association Education Trust (to D.J.L.-S.), the HélioBiotec platform, funded by the European Union (European Regional Development Fund), the Région Provence Alpes Côte d'Azur, the French Ministry of Research, and the Commissariat à l'Energie Atomique.

[2] These authors contributed equally to the article.

* Address correspondence to allahve@utu.fi.

The author responsible for distribution of materials integral to the findings presented in this article in accordance with the policy described in the Instructions for Authors (www.plantphysiol.org) is: Yagut Allahverdiyeva (allahve@utu.fi).

Y.A. designed the research; M.E., T.H., P.R., and L.B. performed the experiments and analyzed the data; C.J.H. and G.P. contributed to the analytical tools; D.J.L.-S. contributed to the data analysis and analytical tools; M.E., T.H., D.J.L.-S., and Y.A. wrote the article.

[OPEN] Articles can be viewed without a subscription.

www.plantphysiol.org/cgi/doi/10.1104/pp.16.00479

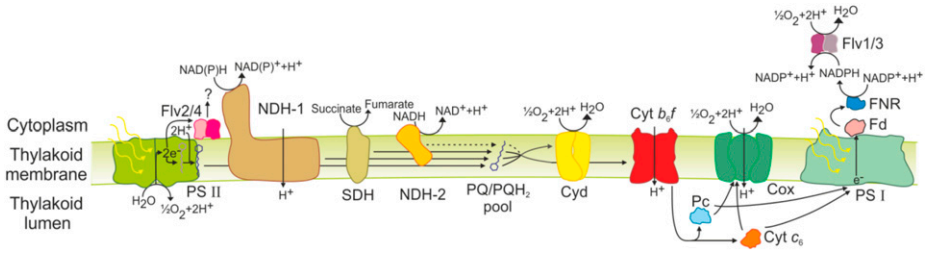

Figure 1. Schematic diagram of the thylakoid membrane-localized photosynthetic and respiratory electron transfer chains. Lines indicate electron transport; dotted lines indicate possible but poorly characterized electron transfer and proton pathways. Cox, Cytochrome *c* oxidase; Cyd, cytochrome *bd* quinol oxidase; Cyt c_6, cytochrome c_6; Fd, ferredoxin; Flv2/4, flavodiiron proteins 2/4; Flv1/3, flavodiiron proteins 1/3; FNR, ferredoxin-NADP$^+$ oxidoreductase; NDH-1, NAD(P)H dehydrogenase-like complex type 1; NDH-2, NAD(P)H dehydrogenase type 2; Pc, plastocyanin; PQ, plastoquinone; PQH_2, plastoquinol; SDH, succinate dehydrogenase.

lumen, and extraction of electrons for the reduction of $P680^+$. Electrons ejected from P680, the primary donor of PSII, are forwarded to pheophytin, then to PQ molecules, Q_A and Q_B. Following double reduction and protonation, PQH_2 diffuses from the Q_B pocket into the membrane. PQH_2 is oxidized by Cyt b_6f, resulting in proton translocation to the lumen and electron transfer to the lumen-localized soluble electron carriers, Pc and Cyt c_6. These small proteins donate electrons to $P700^+$, the oxidized primary electron donor of PSI. Electrons extracted from P700 during charge separation are transferred via a chain of cofactors incorporated in PSI to ferredoxin, a soluble electron carrier on the cytosolic side of the thylakoid membrane. The ferredoxin:NADP$^+$ oxidoreductase concludes the linear electron transport chain by catalyzing the formation of NADPH. A proton gradient established during photosynthetic electron transfer is used by ATP synthase for the production of ATP.

In the model cyanobacterium *Synechocystis* sp. PCC 6803 (hereafter *Synechocystis*), the thylakoid membrane is the site not just of photosynthesis but also of respiration (for review, see Vermaas, 2001; Mullineaux, 2014a; Lea-Smith et al., 2016). The respiratory electron transfer chain transfers electrons extracted from organic molecules into the PQ pool. NAD(P)H dehydrogenase-like complex type 1 (NDH-1), succinate dehydrogenase (SDH), and possibly one to three different NDH-2s may participate in PQ pool reduction (Mi et al., 1992; Howitt et al., 1999; Cooley et al., 2000; Ohkawa et al., 2000). PQH_2 oxidation can then occur via either Cyt b_6f or respiratory terminal oxidases (RTOs). In *Synechocystis*, the cytochrome *bd* quinol oxidase (Cyd), encoded by *cydAB*, reduces oxygen with electrons presumably taken directly from the PQ pool (Berry et al., 2002). Although Cyd does not pump protons across the membrane, it contributes to the thylakoid membrane potential by releasing protons from PQH_2 oxidation into the lumen and by generating water using protons removed from the cytoplasm (for review, see Hart et al., 2005). The aa_3-type cytochrome *c* oxidase (Cox) complex, encoded by *coxBAC*, is situated only in the thylakoid membrane and can accept electrons from Pc and Cyt c_6 (Howitt and Vermaas, 1998; Nomura et al., 2006; Lea-Smith et al., 2013). Therefore, Cyt b_6f, the PQ pool, and Pc/Cyt c_6 are shared by both the photosynthetic and respiratory electron transfer chains (Scherer, 1990). Cox is present in all cyanobacteria sequenced thus far (Pils and Schmetterer, 2001; Lea-Smith et al., 2013). Based on similarity with better characterized aa_3-type Cox complexes from other bacteria, Cox can potentially couple the transfer of electrons to oxygen with the translocation of protons across the membrane (Iwata et al., 1995; Brändén et al., 2006).

An additional electron transport chain is localized in the cytoplasmic membrane, which lacks Cox (Huang et al., 2002) and Cyt b_6f (Schultze et al., 2009). This simpler pathway consists of electrons donated to PQ by NDH-2 and/or SDH, followed by transfer from PQH_2 to RTOs. Localization of Cyd in the thylakoid membrane has been confirmed, but this complex also may be present in the cytoplasmic membrane (Howitt and Vermaas, 1998; Berry et al., 2002). Another RTO, the alternative oxidase complex (ARTO), encoded by *ctaCIIDIIEII*, probably oxidizes the PQ pool and has been localized only to the cytoplasmic membrane in *Synechocystis* (Huang et al., 2002; Pisareva et al., 2007). Thus, ARTO does not have a significant impact on photosynthetic electron transfer (Abramson et al., 2000; Lea-Smith et al., 2013). However, a recent study suggested a possible role for ARTO in reductive iron uptake (Kranzler et al., 2014). An additional quinol oxidase, which is closely related to the plastid terminal oxidase (PTOX) of plants, has been identified in a range of cyanobacteria but is not present in *Synechocystis* (McDonald et al., 2011).

The main role of RTOs is to provide metabolic energy required during dark periods (Matthijs and Lubberding, 1988). RTOs are not essential in *Synechocystis* when cells are subjected to continuous moderate or high light (Howitt and Vermaas, 1998; Pils and Schmetterer, 2001; Lea-Smith et al., 2013) or 12-h-dark/12-h-moderate light (40 μmol photons m^{-2} s^{-1}) cycle regimes (Lea-Smith et al., 2013). However, the presence of Cox is essential for viability under low light (Kufryk and Vermaas, 2006), and the presence of at least one

thylakoid-based RTO (Cyd or Cox) is required for survival under a 12-h-dark/12-h-high light (150 μmol photons m^{-2} s^{-1}) square cycle regime (Lea-Smith et al., 2013).

Studies of RTO mutants by gas exchange under light are complicated in oxygenic photosynthetic organisms due to the oxygen-evolving activity of PSII and the existence of other processes capable of oxygen photoreduction. The Flavodiiron proteins Flv1 and Flv3 are responsible for the majority of oxygen uptake in the light in cyanobacteria (Helman et al., 2003, 2005; Allahverdiyeva et al., 2011; Ermakova et al., 2014). These proteins likely form a functional couple (Flv1/3) and reduce oxygen directly to water, conceivably using NADPH formed as a result of linear electron transfer (Vicente et al., 2002; Helman et al., 2003). Moreover, cyanobacteria possess an active photorespiratory metabolism (Eisenhut et al., 2006, 2008), and photorespiratory oxygen uptake plausibly contributes to the total oxygen uptake in the light and in particular during inorganic carbon limitation (Allahverdiyeva et al., 2011). Therefore, the roles of individual RTOs and their relative importance compared with other electron sinks under light conditions are poorly studied. In this work, we used the wild type and various mutants of *Synechocystis* in combination with specific inhibitors targeting electron transfer chain components to address the role of RTOs in the light. We demonstrate that Cyd is the key RTO under light, capable of light-induced oxygen uptake under suboptimal conditions. By contrast, Cox is responsible for the majority of dark respiration but also can contribute to the regulation of electron flow to PSI under light in specific cases.

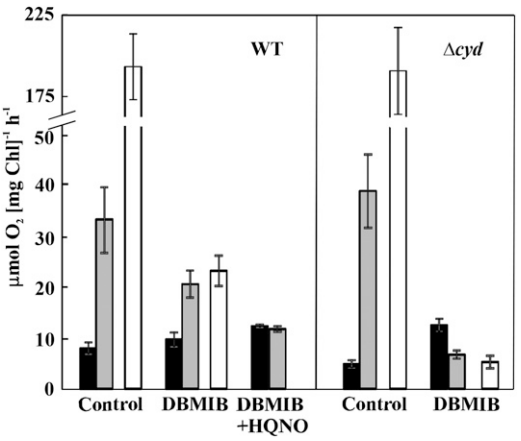

Figure 2. Rates of oxygen exchange in wild-type (WT) and Δ*cyd* mutant cells incubated in darkness for 5 min and then illuminated with a strong white light (400 μmol photons m^{-2} s^{-1}) for the next 5 min. Black bars and gray bars indicate the rates of total oxygen uptake by cells in darkness and in the light, respectively; white bars indicate the gross oxygen production rate. Measurements were performed either in the absence of inhibitors (control) or in the presence of 2,5-dibromo-6-isopropyl-3-methyl-1,4-benzoquinone (DBMIB) or DBMIB + 2-*N*-heptyl-4-hydroxyquinoline *N*-oxide (HQNO). Values are means ± SD; $n = 3$ to 5.

RESULTS

Light-Induced Oxygen Uptake in *Synechocystis* Cells in the Absence and Presence of Inhibitors

For a precise study of oxygen uptake in *Synechocystis* cells, we used membrane inlet mass spectrometry (MIMS) and $^{18}O_2$-enriched oxygen. In contrast to a classical oxygen electrode, which only measures net oxygen production under illumination, MIMS analysis can differentiate between gross oxygen produced by PSII and oxygen uptake under illumination based on increase of $^{16}O_2$ and decrease of $^{18}O_2$, respectively, in the reaction medium. When oxygen exchange was monitored in cultures during the dark-to-light (400 μmol photons m^{-2} s^{-1}) transition, the wild type demonstrated strong oxygen uptake of 34.6 ± 6.7 μmol oxygen mg^{-1} chlorophyll [Chl] h^{-1} under illumination, which was drastically higher than the oxygen uptake of the cells in darkness (8.3 ± 1.2 μmol oxygen mg^{-1} Chl h^{-1}; Fig. 2; averaged values and SDs are provided in Table I; Supplemental Fig. S1). The difference between light and dark oxygen uptake rates is defined as the light-induced oxygen uptake rate. The Δ*flv1/3* mutant lacking the Flv1 and Flv3 proteins demonstrated a slightly higher oxygen uptake rate in darkness than the wild type (10.8 ± 1.6 μmol oxygen mg^{-1} Chl h^{-1}) and a similar oxygen uptake rate in the light to that in darkness (Supplemental Fig. S1). Thus, a strong light-induced oxygen uptake component observed in the wild type was missing in the Δ*flv1/3* mutant. This was in line with previous reports, demonstrating that oxygen uptake in wild-type *Synechocystis* was strongly stimulated in the light due to Flv1/3 activity occurring downstream of PSI (Helman et al., 2003, 2005; Allahverdiyeva et al., 2011, 2013, Mustila et al., 2016).

To investigate a possible role of RTOs functioning at the PQ pool level and to exclude any contribution of Flv1/3 to light-induced oxygen uptake, we performed MIMS experiments in the presence of DBMIB, an inhibitor of PQH_2 oxidation at the site of Cyt b_6f (Draber et al., 1970; Yan et al., 2006). In wild-type cells, in the presence of DBMIB, the dark oxygen uptake rate was 10.1 ± 1.5 μmol oxygen mg^{-1} Chl h^{-1}, whereas in the light, the rate of total oxygen uptake was 2-fold higher than that in darkness (21.1 ± 2.8 μmol oxygen mg^{-1} Chl h^{-1}; Fig. 2; Table I). This demonstrates that a strong light-induced oxygen uptake occurs in wild-type cells in the presence of DBMIB. To clarify the origin of this oxygen uptake, we supplemented the cells, in addition to DBMIB, with 2,6-dichloro-*p*-benzoquinone (DCBQ), an artificial acceptor of electrons from PSII (Graan and Ort, 1986). Under these conditions, light-induced oxygen uptake was completely eliminated (Supplemental Fig. S2A), implying strong competition between DCBQ and an unknown acceptor that can mediate the light-driven flow of electrons to oxygen.

Table I. *Oxygen exchange rates of wild-type and mutant cells*

Rates are in μmol oxygen mg^{-1} Chl h^{-1}. Values are means ± SD, $n = 3$ to 5. Asterisks indicate statistically significant differences compared with the wild type ($P < 0.05$). N/A, not applicable.

Conditions	Parameters	Components	Wild Type	Δ*cyd*	Δ*cox*	Δ*cox/cyd*
Control	Oxygen uptake	Dark	8.3 ± 1.2	5.1 ± 0.8*	3.5 ± 0.5*	0.3 ± 0.2*
		Light induced	26.3 ± 6.9	35.3 ± 8.3*	38.4 ± 5.5*	24.7 ± 3.0
		Total light	34.6 ± 6.7	40.5 ± 7.5	41.5 ± 5.1*	24.9 ± 3.0
	Oxygen production	Gross	193.3 ± 20.1	190.7 ± 26.4	190.25 ± 18.1	184.9 ± 21.5
		Net	158.6 ± 19.3	150.3 ± 19.2	148.7 ± 15.1	159.6 ± 22.5
DBMIB	Oxygen uptake	Dark	10.1 ± 1.5	13.1 ± 1.3	12.8 ± 3.1	9.3 ± 1.3
		Light induced	11.6 ± 2.3	N/A	7.9 ± 0.6 *	N/A
		Total light	21.5 ± 2.8	7.0 ± 0.8*	20.7 ± 2.5	7.7 ± 1.9*
	Oxygen production	Gross	24.2 ± 3.1	5.5 ± 1.3*	19.8 ± 3.8*	2.75 ± 0.4*
		Net	2.9 ± 0.2	N/A	N/A	N/A
DBMIB + HQNO	Oxygen uptake	Dark	12.9 ± 0.3	11.3 ± 3.5	10.9 ± 3.9	10.2 ± 0.2*
		Light induced	N/A	N/A	N/A	N/A
		Total light	12.3 ± 0.6	7.0 ± 1.1	10.8 ± 3.4	9.8 ± 0.5

Importantly, in the presence of DBMIB, the gross oxygen evolution rate of wild-type cells decreased significantly (from 193.3 ± 20.1 μmol oxygen mg^{-1} Chl h^{-1} in the control cells to 24.2 ± 3.1 μmol oxygen mg^{-1} Chl h^{-1}; Fig. 2; Table I), becoming nearly equal to the total oxygen uptake rate under the light. Consequently, the rate of net photosynthesis in the presence of DBMIB was close to zero (Table I).

Next, we used HQNO, an inhibitor of Cyd (Pils et al., 1997). Supplementation of the DBMIB-treated cells with HQNO also completely eliminated the light-induced component of oxygen uptake (Fig. 2; Table I). Thus, the rate of oxygen uptake was observed to be similar between darkness and light, suggesting that Cyd is responsible for the light-induced fraction of oxygen uptake under the studied conditions. The addition of HQNO alone to the wild-type cells did not significantly affect total oxygen uptake under light (Supplemental Fig. S2B), presumably due to the compensatory effect of other oxygen-consuming pathways, such as Cox and Flv1/3.

It is important to note that the addition of DBMIB also increased dark oxygen uptake in wild-type *Synechocystis* cells (from 8.3 ± 1.2 to 10.1 ± 1.5 μmol oxygen mg^{-1} Chl h^{-1}; Table I), which is in line with a previous report (Zhang et al., 2013). This result raises the question of whether DBMIB itself could act as an electron shuttle to oxygen (Bukhov et al., 2003; Belatik et al., 2013), thus making interpretations difficult. In order to clarify the origin of increased oxygen uptake in the presence of DBMIB, the wild-type cells were further treated with KCN, which is an inhibitor of both Cyd and Cox (Howitt and Vermaas, 1998). The addition of KCN to the DBMIB-treated wild-type cells completely abolished the light-induced component of oxygen uptake, suggesting a role for RTOs (Supplemental Fig. S2C). However, oxygen uptake in darkness decreased only slightly in the presence of KCN, demonstrating a residual oxygen uptake with a rate of about 7.4 μmol oxygen mg^{-1} Chl h^{-1} occurring similarly under both darkness and light conditions in DBMIB-supplemented cells (Supplemental Fig. S2C). This suggests the existence of background oxygen uptake in the presence of DBMIB. Importantly, this background oxygen uptake is insensitive to light and, therefore, would not affect the interpretation of light-induced oxygen uptake in the wild type. To clarify further the effect of this compound, we measured oxygen evolution rates of wild-type cells supplemented with different DBMIB concentrations using a Clark-type electrode. With increasing DBMIB concentrations, the net oxygen production decreased gradually to almost zero at a concentration of 25 μM DBMIB (Supplemental Fig. S2D), which is in line with the MIMS experiments (Table I) and suggests that DBMIB acts as an electron transfer inhibitor in *Synechocystis* cells. Our results differ from those of Belatik et al. (2013), who described high oxygen production rates even at low DBMIB concentrations and concluded that DBMIB could act as electron acceptor for PSII in spinach (*Spinacia oleracea*) thylakoids. This discrepancy could be due to different experimental setups and the different organisms used.

Light-Induced Oxygen Uptake in *Synechocystis* Cells Deficient in RTOs

In order to confirm the results obtained with the inhibitors, we subjected mutants deficient in Cyd, Cox, and Cox/Cyd to MIMS analysis, first in the absence of inhibitors (Table I). Dark respiration was reduced in the Δ*cyd* and Δ*cox* mutants and almost abolished in Δ*cox/cyd*. Interestingly, light-induced oxygen uptake was significantly higher in both the Δ*cyd* and Δ*cox* mutants compared with the wild type, presumably due to up-regulation of the other RTO pathway (Fig. 2; Table I). In line with this, Δ*cox/cyd* demonstrated nearly similar light-induced oxygen uptake rates to the wild type. Likewise, the total light oxygen uptake also was increased in the single mutants, whereas a substantial decrease was observed in Δ*cox/cyd* compared with the wild type. All RTO-deficient mutants demonstrated similar gross and net oxygen production rates to wild-type cells (Table I).

In the presence of DBMIB, the rate of dark oxygen uptake was similar between all strains, whereas the light-induced oxygen uptake was completely inhibited in the Δ*cyd* and Δ*cox/cyd* mutants and also significantly reduced in Δ*cox* (Table I). Overall, this resulted in a greatly reduced rate of total oxygen uptake under light in Δ*cyd* and Δ*cox/cyd* but not in Δ*cox*. DBMIB also caused a drastic reduction in gross oxygen production in Δ*cyd* and Δ*cox/cyd*, so that the rates were equal to the total oxygen uptake rates under light, as observed in wild-type cells. The addition of HQNO to the DBMIB-treated cells did not alter oxygen uptake rates in Δ*cyd* cells. Similar to the wild type, the addition of DBMIB and HQNO to Δ*cox* eliminated light-induced oxygen uptake detected in the presence of DBMIB only. These results correlated with the experiments performed on wild-type cells with inhibitors and confirmed that Cyd is responsible for the majority of light-induced oxygen uptake in the presence of DBMIB.

The Impact of RTOs under Fluctuating Light Conditions

It was reported recently that the Δ*flv1/3* mutant exposed to fluctuating light (FL) conditions exhibited extensive damage to PSI, a drastic decrease in net photosynthesis, and a KCN-sensitive component of light-induced oxygen uptake (Allahverdiyeva et al., 2013). To address a possible role of Cyd in light-induced oxygen uptake under FL conditions, MIMS analysis was undertaken in wild-type and Δ*flv1/3* cells incubated under the FL 20/500 regime (20 μmol photons m^{-2} s^{-1} background light interrupted by 30-s pulses of 500 μmol photons m^{-2} s^{-1} light every 5 min) for 3 d. The samples were analyzed either in the absence (control) or presence of HQNO, following illumination of the cells with strong white light of 400 μmol photons m^{-2} s^{-1}. In wild-type cells, the addition of HQNO did not significantly affect the light-induced fraction of oxygen uptake (Fig. 3). Interestingly, the addition of HQNO to Δ*flv1/3* cells acclimated to FL conditions resulted in an 86% inhibition of the light-induced oxygen uptake rate, indicating a significant contribution of Cyd to oxygen uptake in the light.

To investigate further a possible role for Cyd and Cox in the acclimation of cyanobacterial cells to FL, the growth of RTO-deficient mutants was monitored under the FL 20/500 regime for several days. No significant differences were observed in the growth of the mutants compared with wild-type cells (Fig. 4A). Previously, it has been shown and we have also confirmed that the Δ*cox/cyd* double mutant is not viable when subjected to a 12-h-dark/12-h-high light (150 μmol photons m^{-2} s^{-1}) square-wave cycle regime (Lea-Smith et al., 2013; Supplemental Fig. S3A). Interestingly, when the duration of alternating dark and high-light phases was decreased to 5 min (5 min of dark/5 min of high light at 200 μmol photons m^{-2} s^{-1}), the Δ*cox/cyd* mutant survived (Fig. 4B). However, the growth of this strain and of the Δ*cox* mutant was slower after 7 d compared with the wild type and Δ*cyd*.

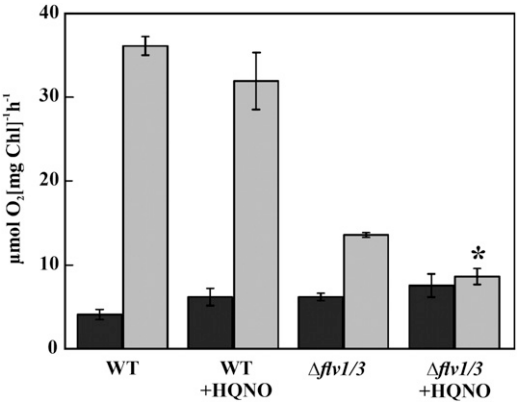

Figure 3. Rates of total oxygen uptake in darkness (black bars) and in the light (gray bars) in the wild type (WT) and Δ*flv1/3* acclimated for 3 d to a fluctuating light FL 20/500 regime (20 μmol photons m^{-2} s^{-1} background light interrupted by 30-s pulses of 500 μmol photons m^{-2} s^{-1} light every 5 min). Measurements were performed using MIMS on cells incubated in darkness for 5 min and then illuminated with a strong white light (400 μmol photons m^{-2} s^{-1}) for 5 min either in the absence (control) or in the presence of HQNO. Values are means ± SD, $n = 3$. The asterisk indicates a statistically significant difference between measurement with HQNO compared with control samples ($P < 0.05$).

Gas-Exchange Analysis of the PSI-Less Mutant

A possible role of RTOs in light-stimulated electron transfer to oxygen in the PSI-less mutant (Shen et al., 1993), which lacks functional PSI, also was studied by MIMS gas-exchange analysis. The ΔPSI cells demonstrated strong light-induced oxygen uptake, which was insensitive to HQNO. However, this could be completely abolished by the addition of KCN (Fig. 5). These results indicated that, in the cells lacking functional PSI, it is not Cyd but Cox that shuttles electrons to oxygen during sudden, strong illumination.

Response of Photosynthesis in RTO-Deficient Mutants to Increasing Light Intensities

To characterize the impact of RTOs on photosynthetic electron transfer, rapid light curves, representing the response of photosynthetic parameters to gradually increasing light intensities, were recorded (Fig. 6). During the experiment, the cells were illuminated with actinic light of different intensities for 60 s, and a saturating pulse was applied at the end of each light period. The Y(II) and the Y(ND) were specifically addressed to monitor the status of the intersystem electron transfer chain. The Δ*cox* mutant was similar to the wild type in the dynamics of Y(II), while Δ*cyd* and Δ*cox/cyd* demonstrated a decrease of Y(II) under increasing light intensities (Fig. 6A). In Δ*cyd* cells, a decrease in PSII yield was observed under light intensities ranging from 57 to 220 μmol photons m^{-2} s^{-1}. The Δ*cox/cyd* double mutant already displayed a decrease in PSII yield at the lower light intensities, starting at 10 μmol photons m^{-2} s^{-1} (Fig. 6A).

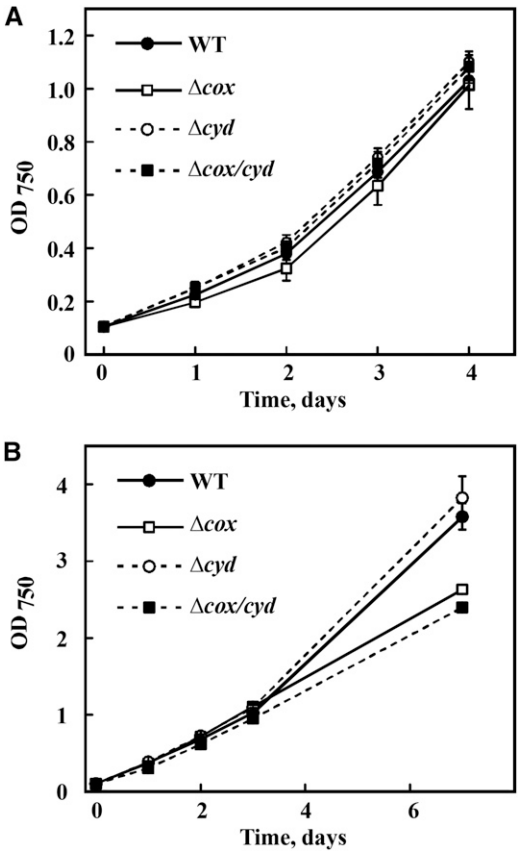

Figure 4. Growth of the *Synechocystis* wild type (WT) and RTO-deficient mutants under FL 20/500 (20 μmol photons m^{-2} s^{-1} background light interrupted every 5 min with 30-s high light pulses of 500 μmol photons m^{-2} s^{-1}; A) or 5-min-dark/5-min-high light (200 μmol photons m^{-2} s^{-1}; B) square-wave cycles monitored by optical density (OD) measurements at 750 nm. Values are means ± SD, $n = 3$.

The dynamics of Y(ND) was again similar between wild-type and Δ*cox* cells: Y(ND) rose gradually as the light intensity increased (Fig. 6B). Interestingly, in Δ*cyd* and Δ*cox/cyd* mutant cells, Y(ND) rose faster than in the wild type and significantly exceeded the wild type values at 58 μmol photons m^{-2} s^{-1} (Fig. 6B). However under higher light intensities, starting from 220 μmol photons m^{-2} s^{-1}, there was a slight but statistically significant difference ($P < 0.05$) in Y(ND) between Δ*cyd* and Δ*cox/cyd*. This result suggests that, under high light, the reduced electron flow to P700 in the Δ*cyd* mutant was presumably due to increased competition for electrons between PSI and Cox. No significant difference between the wild type and RTO-deficient mutants was observed in acceptor side limitation of PSI [Y(NA)] (Supplemental Fig. S4).

To investigate whether the sensitivity of the Cyd-deficient mutants to increasing light intensities would affect the growth of cells under high light, we grew highly diluted cultures of the wild type and RTO-deficient mutants at a continuous light intensity of 500 μmol photons m^{-2} s^{-1} (Supplemental Fig. S3B). None of the mutants exhibited light sensitivity under these conditions, and all cultures reached a similar optical density at 750 nm (OD_{750}) after 2 d of growth.

Analysis of the PQ Pool Redox Status in RTO-Deficient Mutants in Darkness

Next, we studied the PQ pool redox state in RTO-deficient mutants in darkness and under far-red (FR) illumination using Chl fluorescence analysis (Fig. 7). The dark-adapted cells of the wild type, Δ*cox*, and Δ*cyd* demonstrated similar levels of minimal fluorescence (F_0) in the dark, whereas Δ*cox/cyd* cells had a significantly higher F_0 level (Supplemental Table S1). Next, a saturating pulse was applied to the cells to obtain the maximum fluorescence signal in darkness (F_m^D). All strains demonstrated similar F_m^D values (Supplemental Table S1). The double mutant retained a higher level of fluorescence in the dark compared with the wild type, while the Δ*cox* cells exhibited a slower relaxation of saturating pulse-induced fluorescence during the subsequent dark period (Fig. 7).

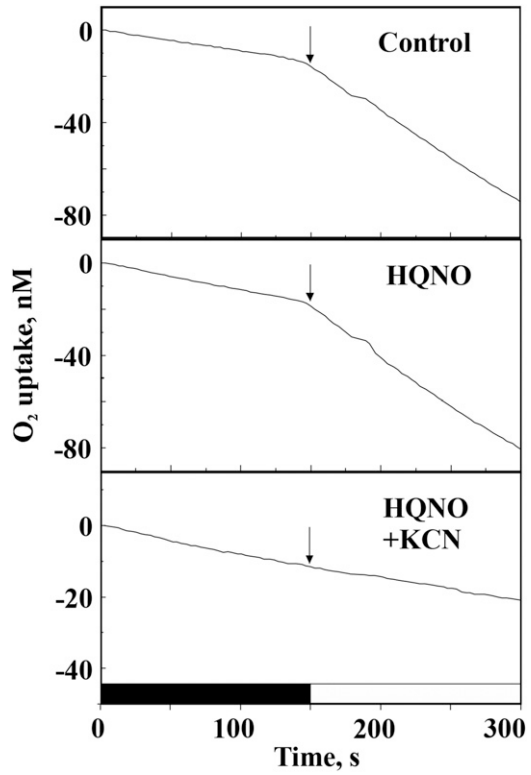

Figure 5. MIMS analysis of oxygen uptake by PSI-less mutant cells in the absence (control) and presence of HQNO and HQNO plus KCN. Oxygen uptake was monitored for 5 min in darkness and 5 min under a light intensity of 150 μmol photons m^{-2} s^{-1}. Arrows indicate the beginning of illumination. The slope of the curves does not provide a precise quantitative measure of the rate of oxygen consumption until it is corrected for the isotopic ratio ($^{16}O/^{18}O$).

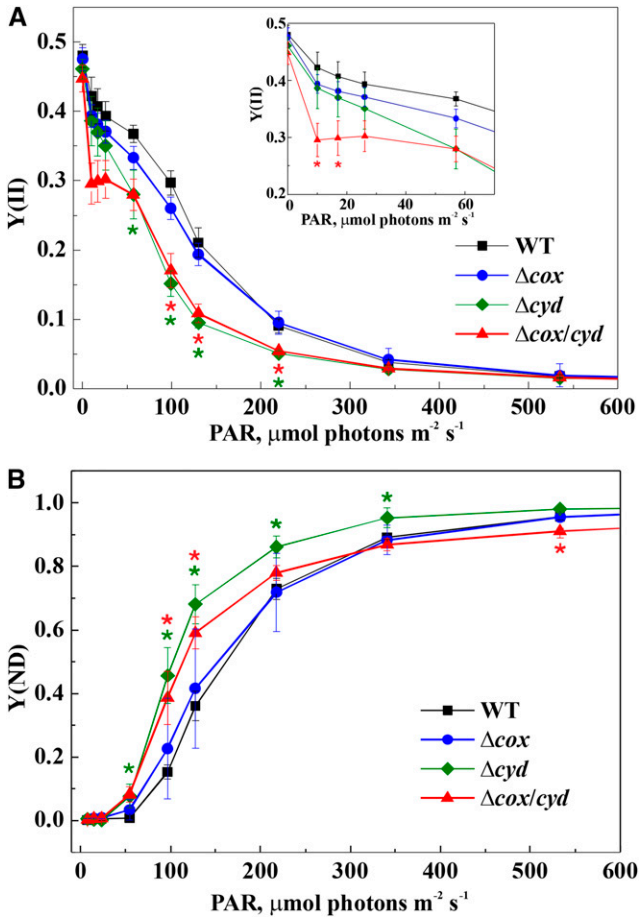

Figure 6. Rapid light curves of the wild type (WT) and RTO-deficient mutants: effective yield of PSII [Y(II); A] and donor side limitation of PSI [Y(ND); B]. Values are means ± SD, $n = 3$. Asterisks indicate statistically significant differences compared with the wild type ($P < 0.05$).

Due to the high flow of electrons to the electron transport chain from respiratory complexes, cyanobacterial cells are usually in state II during dark periods (Mullineaux and Allen, 1986) and, therefore, demonstrate low F_m^D values. In order to induce a state II-to-state I transition, cells were then exposed to FR light for 8 s to preferentially excite PSI and facilitate the oxidation of the PQ pool. FR light application did not affect the fluorescence level in the wild type and single mutants; however, it resulted in a sudden drop of fluorescence in the Δ*cox*/*cyd* double mutant, to a level slightly above those of wild-type and single mutant cells (Fig. 7). The FR light-mediated decrease of fluorescence suggested a highly reduced PQ pool in Δ*cox*/*cyd* cells in darkness, which is in agreement with an earlier study by Howitt et al. (2001). When a saturating pulse was applied over an FR light background, all strains demonstrated an increased maximum fluorescence level (Fig. 7; Supplemental Table S1). Afterward, the relaxation of fluorescence was again recorded in darkness. The fluorescence levels of wild-type and Δ*cyd* cells dropped down to a value similar to their initial F_0 levels. The fluorescence signal of the Δ*cox*/*cyd* mutant immediately returned to its initial higher level, demonstrating rapid reduction of the PQ pool in darkness. The Δ*cox* cells demonstrated only a transient increase and subsequent relaxation of the fluorescence level after the termination of FR illumination.

Characterization of PSII Functional Status in RTO-Deficient Mutants

To analyze in detail the functional status of PSII in the RTO-deficient mutants, the maximum quantum yield of PSII was first measured with the Dual-PAM fluorometer in the presence of 3-(3,4-dichlorophenyl)-1,1-dimethylurea (DCMU). The values did not differ significantly between the wild type and mutants (Supplemental Table S1). This is in line with the MIMS data showing nearly similar gross oxygen production in all studied RTO-deficient mutants compared with the wild type (Table I).

Next, the status of the PSII acceptor and donor sides in these strains was precisely addressed by comparing the relaxation kinetics of the flash-induced fluorescence yield. Following a single-turnover flash, relaxation of the variable fluorescence yield in darkness reflects the Q_A^- reoxidation via forward Q_A-to-Q_B electron transfer and back recombination with $S_{2/3}$ states of the water-oxidizing complex of PSII. The fluorescence relaxation

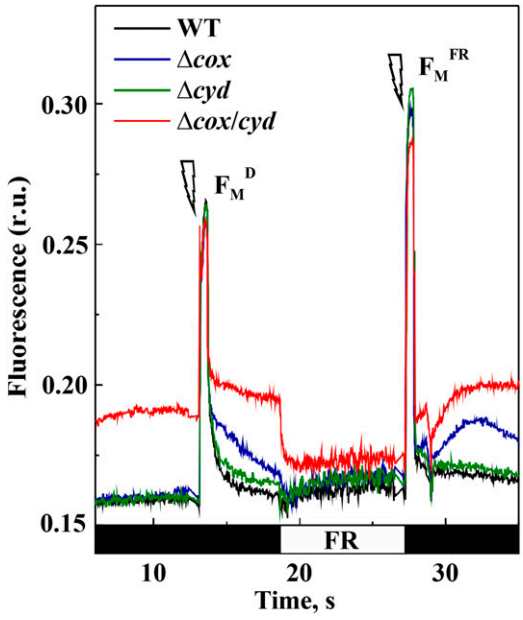

Figure 7. Fluorescence analysis of wild-type (WT) and RTO-deficient mutant cells. Fluorescence was recorded in darkness (F_0; black bars on the time scale) and under far-red (FR) light. Saturating pulses indicated by flashes were fired to monitor F_m^D and maximum fluorescence level under the FR background (F_M^{FR}). The values are provided in Supplemental Table S1. Samples were adjusted to a Chl concentration of 15 μg mL^{-1} and dark adapted for 10 min before the measurements. A representative curve of three independent experiments is shown. r.u., Relative units.

kinetics was comparable for wild-type and Δ*cyd* cells (Supplemental Fig. S5A), while Δ*cox* showed a slower fluorescence decay and the Δ*cox*/*cyd* mutant demonstrated a drastically slower decay (Fig. 8A). These data indicated modified electron transfer at the PSII acceptor side in Δ*cox*, which is exacerbated further in the Δ*cox*/*cyd* mutant cells. Interestingly, the fluorescence relaxation curve of Δ*cox*/*cyd* displayed a slight wave phenomenon, showing a dip at the time point of approximately 50 ms and a transient rise of fluorescence at about 1 s after the flash. Deák et al. (2014) recently observed a similar kinetics of fluorescence relaxation in *Synechocystis* cells when the electron flow to oxygen was inhibited under anoxic conditions. This was due to transient oxidation of the highly reduced PQ pool by PSI, followed by its rereduction from cytosolic components via the NDH-1 complex.

In order to clarify whether the slower relaxation kinetics of the Δ*cox* and Δ*cox*/*cyd* mutants was due to a reduced PQ pool or to structural modifications in the PSII complex, strong FR illumination was applied to cells just before fluorescence measurements. Preillumination of the Δ*cox*/*cyd* cells with FR light, preferentially exciting PSI and thus oxidizing the PQ pool, significantly accelerated the fluorescence decay, bringing the curve closer to that of Δ*cox* cells (Fig. 8A). However, after 10 s of darkness, the fluorescence level of the Δ*cox*/*cyd* cells again started to increase. These results strongly suggest that a slowdown of the Q_A reoxidation rate in Δ*cox*/*cyd* was predominantly due to a highly reduced PQ pool in darkness. However, FR illumination did not significantly affect the fluorescence relaxation kinetics of the Δ*cox* cells (Supplemental Fig. S5B).

In the presence of DCMU, which blocks electron transfer at the Q_B site, Q_A^- reoxidation occurs via charge recombination with the donor side components, mostly the S_2 state of the water-oxidizing complex (Vass et al., 1999). Interestingly, in the presence of DCMU, Δ*cox*/*cyd* still demonstrated slightly slower fluorescence relaxation compared with the wild type, likely indicating the accumulation of PSII centers with a modified donor side in the mutant cells. The Δ*cox* and Δ*cyd* cells showed a similar relaxation kinetics profile to the wild type (Fig. 8B).

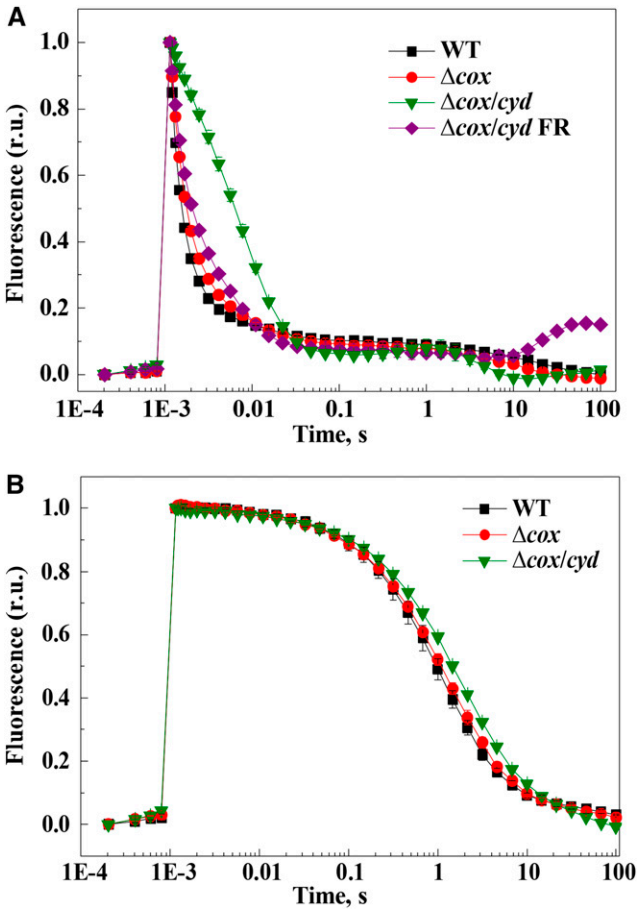

Figure 8. Relaxation of the flash-induced fluorescence yield in darkness. Q_A^- reoxidation was monitored from dark-adapted wild-type (WT; black squares), Δ*cox* (red circles), Δ*cox/cyd* (green diamonds), and Δ*cox/cyd* (purple diamonds) cells preilluminated with FR light for 30 s (A) and in the presence of 20 μM DCMU (B). Values are means ± SD, $n = 3$. The F_0 and F_m values were normalized to 0 and 1, respectively, to facilitate comparison of the kinetics. r.u., Relative units.

The P700 Redox State in the RTO-Deficient Mutants

The redox state of P700 was monitored during dark-light-dark transitions by the application of strong FR light (Fig. 9). The kinetics of P700 oxidation and rereduction was similar between wild-type and Δ*cyd* cells. The Δ*cox* mutant demonstrated a small lag phase during the oxidation of P700 and faster rereduction compared with the wild type. Drastically slower oxidation and faster rereduction were recorded for the Δ*cox*/*cyd* mutant as compared with the wild type and single mutants (Fig. 9). This is in line with the fluorescence analysis results, implying a highly reduced PQ pool in Δ*cox*/*cyd* cells in darkness. However, the maximum amount of oxidizable P700 did not differ significantly between the wild type and RTO-deficient mutants (Supplemental Table S1).

The PSII-PSI Ratio in the RTO-Deficient Mutants

In order to determine whether the modified redox state of the PQ pool observed in the double mutant during dark-to-light transitions affected energy transfer between photosystems, the 77 K fluorescence emission spectra of the wild type and RTO-deficient mutants was analyzed. Spectra of mutant cells excited with either 440-nm (Chl excitation) or 580-nm (phycobilisome excitation) light did not differ from the wild-type spectra (Supplemental Fig. S6), suggesting the absence of significant changes in the PSII-PSI ratio and in energy transfer from phycobilisomes to the reaction centers of photosystems. In addition, total protein fractions were isolated from the cells grown under continuous light

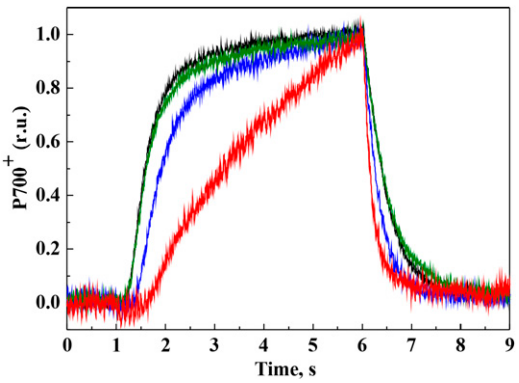

Figure 9. P700 oxidoreduction. P700 oxidation and rereduction in wild-type and mutant cells was illuminated with strong FR light for 5 s. Cells are as follows: wild type (black), Δ*cox* (blue), Δ*cyd* (green), and Δ*cox*/*cyd* (red). Curves were normalized to the same amplitude to facilitate comparison of the kinetics. Representative curves of three independent experiments are shown. r.u., Relative units.

(50 μmol photons m^{-2} s^{-1}) and probed with a range of antibodies. The amount of PsaB and PsbA (D1), proteins in the reaction centers of PSI and PSII, respectively, were similar between all strains (Supplemental Fig. S7). Likewise, amounts of the ATP synthase β-subunit and Flv2, Flv3, and Flv4 were similar between all strains.

DISCUSSION

The intersystem electron transport chain of photosynthetic organisms plays an important role the in regulation of the photosynthetic apparatus. The Cyt b_6f complex in higher plants is known to act in photosynthetic control, regulating electron flow to PSI (Nishio and Whitmarsh, 1993; Joliot and Johnson, 2011; Suorsa et al., 2013). In *Synechocystis*, the presence of thylakoid membrane-localized terminal oxidases, Cyd and Cox, strongly suggests that RTOs may regulate the intersystem electron transport, not only under dark conditions but also during light periods. In *Synechocystis*, the total oxygen uptake in the light could consist of two components: the respiratory component and the light-induced component. The respiratory component can be detected in darkness but also could contribute to the total oxygen uptake observed under light, whereas the light-induced component can only be monitored upon the application of light and is estimated by subtracting the respiratory component from total oxygen uptake under light. Shifting cells from darkness to dim light is known to inhibit oxygen uptake by RTOs (Kok effect), likely because of the higher affinity of PSI for electrons from Pc and Cyt c_6 (Kok, 1949). However, accurately determining the contribution of specific respiratory RTOs to the total oxygen uptake under moderate or high light is a challenge, mainly because it is not known how their relative activity changes under different conditions.

Cyd Contributes to the Redox Poise of the PQ Pool under Light

It was generally accepted that the addition of DBMIB should maintain a reduced PQ pool during periods of illumination by blocking electron transport at the site of Cyt b_6f (Draber et al., 1970; Yan et al., 2006). Therefore, in numerous studies, DCMU or DBMIB was added to cyanobacterial cells in order to simulate either an oxidized or a reduced redox state of the PQ pool (Hihara et al., 2003; Huang et al., 2003). However, recent data obtained via HPLC demonstrated that, in wild-type *Synechocystis* cells, the PQ pool is not as highly reduced during illumination in the presence of DBMIB as previously thought (Schuurmans et al., 2014). Here, we demonstrate that, following the inhibition of linear electron transport with DBMIB, wild-type cells of *Synechocystis* are capable of light-induced oxygen uptake, indicating the presence of an alternative electron exit route from the PQ pool to oxygen in the light (Fig. 2). The observed stimulation of oxygen reduction in the light was completely missing after the addition of HQNO to DBMIB-treated wild-type and Δ*cox* cells as well as in the Δ*cyd* and Δ*cox*/*cyd* cells subjected to DBMIB only (Fig. 2; Table I). Thus, Cyd contributes to the light-induced oxygen uptake observed in the wild type when linear electron transport is limited.

Earlier studies already suggested that Cyd is involved in the oxidation of the PQ pool (Schneider et al., 2001, 2004; Berry et al., 2002). However, those studies were based on an indirect fluorescence method. Through application of the $^{18}O_2$ isotope and the MIMS technique, we could directly demonstrate the oxygen uptake activity of Cyd (Fig. 2) and also confirmed that Cyd accepts electrons directly from the PQ pool, since the addition of DCBQ eliminated Cyd-mediated light-induced oxygen uptake (Supplemental Fig. S2A). In the presence of DBMIB, the rates of total oxygen uptake in the light were similar to the rates of gross oxygen production by PSII. Therefore, the rate of net photosynthesis was close to zero in the wild type and the single mutants (Table I). Importantly, the gross oxygen production rates were about 4 times higher in the wild-type and Δ*cox* cells compared with Δ*cyd* and Δ*cox*/*cyd*, suggesting that the quinol-oxidizing activity of Cyd contributes to the alleviation of PSII acceptor side limitation and facilitates gross oxygen production in the presence of DBMIB. This is corroborated by earlier reports that demonstrated an increased level of Cyd associated with an impairment of the Cyt b_6f complex in mutants lacking LepB1 and PetC1 (Tsunoyama et al., 2009; Zhang et al., 2013).

A decrease of the effective PSII yield in the Δ*cyd* and Δ*cox*/*cyd* mutant cells upon a sudden increase in light intensity indicates that, in the absence of Cyd, electrons accumulate in the PQ pool and affect the Y(II) levels (Fig. 6A). These data also demonstrate that PQH_2 oxidation by Cyt b_6f is the rate-limiting step in the linear electron transport under suboptimal conditions. Conservation of the PQH_2 oxidizing terminal oxidases, Cyd, ARTO, or PTOX, in all sequenced cyanobacteria

that are potentially exposed to high light further emphasizes the importance of an alternative electron exit pathway to that provided by Cyt b_6f (Lea-Smith et al., 2013). An example occurs in the marine cyanobacterium *Synechococcus* WH8102, which exhibits a significant flow of electrons to oxygen, likely via PTOX, and is caused by the highly reduced state of the PQ pool due to the shortage of Cyt b_6f and PSI in an iron-limited environment (Bailey et al., 2008). Moreover, Δ*cyd* develops high PSI donor side limitation more rapidly under elevated light intensities (Fig. 6B), due to upregulated Cox activity, as shown by the increased light-induced oxygen uptake rate in this strain (Table I). Previous studies also suggest that the activity of RTOs in the light might be regulated by the redox state of Pc and Cyt *c* (in the case of Cox) and, plausibly, by the redox state of the PQ pool (in the case of Cyd, PTOX, and possibly ARTO; Ardelean and Peschek, 2011).

Interplay between Cyd and Flavodiiron Proteins

It is clear that both Flv1 and Flv3 are responsible for the light-induced oxygen uptake in *Synechocystis* at least during dark-to-high light transitions (Supplemental Fig. S1; Helman et al., 2003; Allahverdiyeva et al., 2011). Helman et al. (2005) estimated that, in low-CO_2-grown cells of Δ*flv3*, RTOs redirect 6% of electrons originating from water splitting to oxygen in the light. Thus, upon the application of strong light, the mutant retains the respiratory component of oxygen uptake driven by RTOs as an alternative sink for light-driven electrons. In agreement with this, under FL conditions, where the electron transfer chain is drastically inhibited in Δ*flv1/3* due to damage to PSI (Allahverdiyeva et al., 2013), the Δ*flv1/3* mutant showed an HQNO-sensitive light-induced oxygen uptake (Fig. 3). This is yet another demonstration of Cyd-driven light-induced oxygen uptake when cells are grown under suboptimal conditions, despite the absence of changes in *cyd* transcript level under FL (Mustila et al., 2016).

It was reported previously that light-induced oxygen uptake in the Δ*flv1/3* cells under FL functioned at full capacity when cells were exposed to background dim light (20 μmol photons m^{-2} s^{-1}) and that this did not increase further upon the application of high-light pulses. Therefore, Cyd cannot rescue the fatal Δ*flv1/3* phenotype (Allahverdiyeva et al., 2013). The unambiguous importance of Flv1 and Flv3 under FL indicates that they function on a fast time scale downstream of PSI and have a higher capacity as an electron sink under these conditions compared with the RTOs. In part, this could be due to the soluble nature of Flv1 and Flv3, which would facilitate a rapid association with NADPH and allow large amounts of protein to accumulate in the cytosol. In contrast, RTOs are membrane localized and may be limited in number, due to the highly crowded nature of the thylakoid membrane. Following rapid light changes, a time-consuming redistribution of protein complexes occurs within the membrane in order to facilitate efficient electron transfer (Liu et al., 2012; Mullineaux, 2014b).

Cox Is Mostly Active in Dark Respiration and Can Be Substituted by Cyd under Light Conditions

The contribution of Cyd to dark respiration seems to be minor, since the redox state of the PQ pool in Δ*cyd* cells was not affected in darkness, as confirmed via P700 oxidoreduction (Fig. 9), Q_A^- reoxidation kinetics (Fig. 8; Supplemental Fig. S5), and fluorescence analysis (Fig. 7). However, the presence of Cyd was beneficial in Δ*cox* cells under light, since Q_A^- reoxidation and the P700 oxidoreduction kinetics differed significantly between Δ*cox* and Δ*cox/cyd* cells (Figs. 8 and 9). In contrast to Δ*cyd*, deletion of Cox drastically decreased the rate of dark respiration (Table I; Pils et al., 1997; Howitt and Vermaas, 1998; Pils and Schmetterer, 2001) and had a prominent effect on the redox state of the PQ pool in darkness (Figs. 7–9) but not under illumination (Fig. 6). Therefore, in *Synechocystis*, Cox can be efficiently substituted by Cyd under illumination. Nevertheless, in the PSI-less mutant of *Synechocystis*, Cox instead of Cyd was the main RTO shuttling electrons to oxygen in the light (Fig. 5). Since Cox is required for chemoheterotrophic growth of *Synechocystis* (Pils et al., 1997) and the PSI-less mutant grows in the presence of Glc under a low light intensity of 5 μmol photons m^{-2} s^{-1}, it is highly possible that Cox is the main thylakoid-localized RTO in this mutant. However, since the PSI-less mutant is highly sensitive to light (Shen et al., 1993), the contribution of Cox as an electron shuttle to oxygen is likely to be less efficient compared with PSI activity, or this could be a transient phenomenon. It is possible that, under specific conditions, Cox also produces reactive oxygen species via a mechanism similar to PTOX in plants (Heyno et al., 2009; Feilke et al., 2014; Yu et al., 2014), thereby generating oxidative damage to the cells. On the other hand, rapid light curve analysis demonstrated a slight but significant difference in Y(ND) values between Δ*cyd* and Δ*cox/cyd* cells under higher light intensities, indicating competition between PSI and Cox for electrons in the Δ*cyd* mutant (Fig. 6B). Thus, both Cyd and Cox have a role in regulating the amount of electrons arriving to PSI in the light, although Cox activity increases only in the absence of Cyd.

The Role of RTOs in Dark/Light Transitions

Despite strong evidence for thylakoid-based RTOs regulating photosynthetic electron flow, deletion mutants do not demonstrate a strong photoautotrophic growth phenotype under continuous moderate light (Howitt and Vermaas, 1998; Lea-Smith et al., 2013), high light (Supplemental Fig. S3B; Lea-Smith et al., 2013), and FL (Fig. 4A) intensity regimes. Thus, it is likely that when the Flv1/3 complex is functioning properly under illumination, RTOs are not essential. However, during periods of darkness, only RTOs can

oxidize the PQ pool, as demonstrated by the Δ*cox*/*cyd* mutant having a drastically slower oxidation and faster rereduction rate of P700 and slower Q_A^- reoxidation kinetics in the dark (Figs. 7–9). Importantly, the PQ pool in the double mutant could be immediately oxidized by the application of strong FR light (Figs. 7 and 8) but not by the application of low light. The latter result could be concluded from a decreased Y(II) in the light curve analysis at 10 to 30 μmol photons m^{-2} s^{-1} light intensity (Fig. 6A). However, in the same experiment under moderate and high light intensities, Δ*cox*/*cyd* behaved similarly to the Δ*cyd* cells.

Either Cox or Cyd is required for the survival of cells under 12-h-high light/12-h-dark square-wave cycles (Supplemental Fig. S3A; Lea-Smith et al., 2013) but interestingly not under 12-h-high light/12-h-dark sinusoidal-wave cycles (Lea-Smith et al., 2013) or 5-min-high light/5-min-dark square-wave cycles (Fig. 4B). Therefore, the importance of RTOs seems to depend on both the length of the dark and light periods and the amount of photodamage occurring during the light period. Indeed, significant reactive oxygen species production and inactivation of the PSII complex were observed in the double mutant subjected to 12-h-high light/12-h-dark square-wave cycles only at the end of a long dark period, possibly due to an insufficient amount of ATP for PSII repair and an overreduced PQ pool (Lea-Smith et al., 2013). Under 12-h-high light/12-h-dark sinusoidal-wave cycles, (1) cells are not subjected to rapid high-light exposure, reducing damage to PSII, and moreover (2) damaged PSII centers have a possibility for efficient repair during a low-light phase before a dark period; therefore, the cells have a reduced energy requirement for repair, which can be substituted by alternatives to dark respiration, most likely fermentation.

Under short dark/light periods (Fig. 4B), the cells may be able to oxidize the PQ pool regularly, thus generating ATP and reducing power that can be used in darkness, although not as efficiently as the wild type, since growth of the Δ*cox* and Δ*cox*/*cyd* mutants was reduced after 7 d.

CONCLUSION

Through the use of well-defined mutants and inhibitors combined with MIMS gas-exchange analysis, we show the subtle effects of the loss of RTO complexes on each part of the photosynthetic electron transfer chain. Importantly, RTO-mediated respiratory oxygen uptake can continue at a similar rate upon high-light illumination, thus contributing to oxidation of the PQ pool. Cox is the most important RTO in dark respiration, but it also competes with PSI for electrons, functioning as a regulator of the electron flow to this photosystem under high light. Under illumination, Cyd is the major RTO oxidizing PQH_2. However, Cyd only up-regulates oxygen photoreduction under certain conditions, specifically when Flv1 and Flv3 protein activity is insufficient to prevent linear electron transport blockage at the level of Cyt b_6f or PSI. Flv1 and Flv3 proteins are not involved in dark respiration but are responsible for the majority of the light-induced oxygen uptake component. Thus, both RTOs and Flv1/3 pathways play an important role in the alleviation of excess electrons using oxygen as a terminal acceptor under illumination: RTOs continue to function in the light, although operating on slower time ranges and on a limited scale, whereas Flv1/3 responds rapidly as a light-induced component and with greater capacity.

MATERIALS AND METHODS

Strains and Culture Conditions

The strains used in this study included *Synechocystis* sp. PCC 6803 (wild type); mutants lacking respiratory terminal oxidases: Δ*cyd*, Δ*cox*, and Δ*cox*/*cyd* (all described previously by Lea-Smith et al. [2013]); mutant deficient in flavodiiron proteins: Δ*flv1*/*flv3* (Allahverdiyeva et al., 2011); and the PSI-less mutant (Shen et al., 1993). Cells were maintained in BG11 medium buffered with 10 mM TES-KOH (pH 8.2) under continuous illumination of 50 μmol photons m^{-2} s^{-1} (photosynthetically active radiation), 3% CO_2, and 30°C with gentle agitation (120 rpm). For all physiological experiments, cells were inoculated to OD_{750} = 0.5 to 0.6 and shifted to ambient CO_2 conditions for 3 d before measurements. Experimental cultures were cultivated in AlgaeTron AG130 growth chambers (PSI Instruments) under continuous illumination of 50 μmol photons m^{-2} s^{-1} (provided by cool-white light-emitting diodes), unless mentioned otherwise. For the high-light growth experiments, a dilution series of cells starting from OD_{750} = 0.1 were subjected to a light intensity of 500 μmol photons m^{-2} s^{-1}. For the MIMS measurements of FL-treated cells, cultures at OD_{750} = 0.5 to 0.6 were shifted to a light regime with a background light of 20 μmol photons m^{-2} s^{-1} interrupted by 30-s pulses of 500 μmol photons m^{-2} s^{-1} light every 5 min (FL 20/500). For the growth experiments under FL conditions, cells were subjected to FL 20/500 or a 5-min-dark/5-min-high light (200 μmol photons m^{-2} s^{-1}) light regime starting from OD_{750} = 0.1. For all activity measurements, cells were harvested and resuspended in fresh BG11 medium at the desired Chl concentration and acclimated for 1 h under the respective growth conditions before the measurements. The PSI-less mutant was grown in the presence of 5 mM Glc at a light intensity of 5 μmol photons m^{-2} s^{-1}. Oxygen evolution measurements with Clark-type electrode are described in detail in Supplemental Methods S1.

MIMS

Online measurements of $^{16}O_2$ (mass 32) production and $^{18}O_2$ (mass 36) consumption were monitored using mass spectrometry (model Prima PRO; Thermo Scientific). The membrane inlet system consists of a thermo-regulated DW1 oxygen electrode chamber, which is connected to the vacuum line of the mass spectrometer via a gas-permeable thin Teflon membrane (1 mm stretch membrane; YSI), which seals the bottom of the chamber. For analyses, 1.5 mL of cell suspension at a Chl concentration of 15 μg mL^{-1} was placed into the measuring chamber and stirred continuously. Gases dissolved in the medium diffuse through the Teflon membrane to the ion source of the mass spectrometer. Prior to the measurement, $^{18}O_2$ (isotope purity greater than 98%; CK Gas Products) was injected by bubbling at the top of the suspension until the concentrations of $^{16}O_2$ and $^{18}O_2$ were equal. Then, samples were measured for 5 min in darkness to record oxygen consumption caused by respiration. Following this period, actinic light (400 μmol photons m^{-2} s^{-1}, or 150 μmol photons m^{-2} s^{-1} in the case of the PSI-less mutant) was applied via a 150-W, 21-V EKE quartz halogen-powered fiber optic illuminator (Fiber-Lite DC-950; Dolan-Jenner). Gas-exchange kinetics and rates were determined according to Beckmann et al. (2009). The final concentrations of inhibitors and electron acceptors used in MIMS experiments were 25 μM DBMIB, 50 μM HQNO, 0.5 mM DCBQ, and 1 mM KCN. All the measurements were performed in the presence of 1 mM $NaHCO_3$.

Protein Isolation, Electrophoresis, and Immunodetection

Total protein extracts of *Synechocystis* cells were isolated as described by Zhang et al. (2009). Proteins were separated by 12% (w/v) SDS-PAGE

containing 6 M urea, transferred to a polyvinylidene difluoride membrane (Immobilon-P; Millipore), and analyzed with protein-specific antibodies.

Fluorescence Measurements

The Chl fluorescence from intact cells was recorded with a pulse amplitude-modulated fluorometer (Dual-PAM-100; Walz). Prior to measurements, cell suspensions at a Chl concentration of 15 μg mL^{-1} were dark adapted for 10 min. Saturating pulses of 5,000 μmol photons m^{-2} s^{-1} (300 ms) and strong FR light (720 nm, 75 W m^{-2}) were applied to samples when required. The maximum quantum yield of PSII was calculated as $(F_m - F_0)/F_m$ where F_m is a maximum level of fluorescence, measured in the presence of 20 μM DCMU from dark-adapted cells upon the application of red actinic light of 200 μmol photons m^{-2} s^{-1} for 1 min.

The kinetics of the Chl fluorescence decay after a single-turnover saturating flash was monitored using an FL 3500 fluorometer (PSI Instruments) according to Vass et al. (1999). Cells were adjusted to a Chl concentration of 7.5 μg mL^{-1} and dark adapted for 5 min before measurements. When indicated, measurements were performed in the presence of 20 μM DCMU. In some experiments, cells were illuminated for 30 s with a strong FR light before application of the flash.

The fluorescence emission spectra at 77 K were measured from intact cells using a USB4000-FL-450 spectrofluorometer (Ocean Optics). Samples were removed from cultures, adjusted to a Chl concentration of 7.5 μg mL^{-1}, rapidly frozen in liquid nitrogen, and excited with 580- or 440-nm light generated with interference filters 10 nm in width.

P700 Oxidation and Rereduction

Oxidation and rereduction of P700 were monitored using a Dual-PAM-100 fluorometer (Walz). Cell suspensions at a Chl concentration of 20 μg mL^{-1} were dark adapted for 2 min before measurements. For P700 oxidation, cells were illuminated with strong FR light (720 nm, 75 W m^{-2}) for 5 s, and the subsequent rereduction was recorded in darkness.

Light Curves

Rapid light curves were measured without dark adaptation of the cells using standard protocols programmed into a Dual-PAM-100 fluorometer (Walz) with the 60-s illumination periods gradually increasing in light intensity. At the end of each light period, a saturating pulse was applied to monitor the photosynthetic parameters. Y(II) was calculated as $(F_m' - F_s)/F_m'$. Y(ND) was calculated as P/P_m. Y(NA) was calculated as $(P_m - P_m')/P_m$. F_m', the maximal level of fluorescence under light; Fs, the level of steady-state fluorescence under light; P, the level of P700 signal under light; P_m, the maximum level of oxidizable P700; P_m', the maximum level of oxidizable P700 under light.

Supplemental Data

The following supplemental materials are available.

Supplemental Figure S1. MIMS analysis of oxygen uptake by wild-type and Δ*flv1/3* cells during the dark-to-light transition.

Supplemental Figure S2. Rates of oxygen uptake and oxygen production in wild-type *Synechocystis* cells.

Supplemental Figure S3. Growth of *Synechocystis* wild-type and RTO-deficient mutant cells under different light conditions.

Supplemental Figure S4. Y(NA) of the wild type and RTO-deficient mutants calculated from the rapid light curves.

Supplemental Figure S5. Relaxation of the flash-induced fluorescence yield from the wild type and RTO mutants.

Supplemental Figure S6. Fluorescence emission spectra recorded at 77 K.

Supplemental Figure S7. Protein analysis of wild-type *Synechocystis* and RTO-deficient mutants.

Supplemental Table S1. Photosynthetic parameters of the wild type and RTO-deficient mutants.

Supplemental Methods S1. Oxygen evolution measurements with a Clark-type oxygen electrode.

ACKNOWLEDGMENTS

We thank Dr. W. Vermaas for sharing the PSI-less mutant.

Received March 25, 2016; accepted April 11, 2016; published April 18, 2016.

LITERATURE CITED

Abramson J, Riistama S, Larsson G, Jasaitis A, Svensson-Ek M, Laakkonen L, Puustinen A, Iwata S, Wikström M (2000) The structure of the ubiquinol oxidase from Escherichia coli and its ubiquinone binding site. Nat Struct Biol **7:** 910–917

Allahverdiyeva Y, Ermakova M, Eisenhut M, Zhang P, Richaud P, Hagemann M, Cournac L, Aro EM (2011) Interplay between flavodiiron proteins and photorespiration in Synechocystis sp. PCC 6803. J Biol Chem **286:** 24007–24014

Allahverdiyeva Y, Mustila H, Ermakova M, Bersanini L, Richaud P, Ajlani G, Battchikova N, Cournac L, Aro EM (2013) Flavodiiron proteins Flv1 and Flv3 enable cyanobacterial growth and photosynthesis under fluctuating light. Proc Natl Acad Sci USA **110:** 4111–4116

Ardelean II, Peschek GA (2011) The site of respiratory electron transport in cyanobacteria and its implication for the photo-inhibition of respiration. *In* GA Peschek, C Obinger, G Renger, eds, Bioenergetic Processes of Cyanobacteria: From Evolutionary Singularity to Ecological Diversity. Springer, New York, pp 131–136

Bailey S, Melis A, Mackey KR, Cardol P, Finazzi G, van Dijken G, Berg GM, Arrigo K, Shrager J, Grossman A (2008) Alternative photosynthetic electron flow to oxygen in marine Synechococcus. Biochim Biophys Acta **1777:** 269–276

Beckmann K, Messinger J, Badger MR, Wydrzynski T, Hillier W (2009) On-line mass spectrometry: membrane inlet sampling. Photosynth Res **102:** 511–522

Belatik A, Joly D, Hotchandani S, Carpentier R (2013) Re-evaluation of the side effects of cytochrome b6f inhibitor dibromothymoquinone on photosystem II excitation and electron transfer. Photosynth Res **117:** 489–496

Berry S, Schneider D, Vermaas WF, Rögner M (2002) Electron transport routes in whole cells of Synechocystis sp. strain PCC 6803: the role of the cytochrome bd-type oxidase. Biochemistry **41:** 3422–3429

Brändén G, Gennis RB, Brzezinski P (2006) Transmembrane proton translocation by cytochrome c oxidase. Biochim Biophys Acta **1757:** 1052–1063

Bukhov NG, Sridharan G, Egorova EA, Carpentier R (2003) Interaction of exogenous quinones with membranes of higher plant chloroplasts: modulation of quinone capacities as photochemical and non-photochemical quenchers of energy in photosystem II during light-dark transitions. Biochim Biophys Acta **1604:** 115–123

Cooley JW, Howitt CA, Vermaas WF (2000) Succinate:quinol oxidoreductases in the cyanobacterium Synechocystis sp. strain PCC 6803: presence and function in metabolism and electron transport. J Bacteriol **182:** 714–722

Deák Z, Sass L, Kiss E, Vass I (2014) Characterization of wave phenomena in the relaxation of flash-induced chlorophyll fluorescence yield in cyanobacteria. Biochim Biophys Acta **1837:** 1522–1532

Draber W, Trebst A, Harth E (1970) On a new inhibitor of photosynthetic electron-transport in isolated chloroplasts. Z Naturforsch B **25:** 1157–1159

Eisenhut M, Kahlon S, Hasse D, Ewald R, Lieman-Hurwitz J, Ogawa T, Ruth W, Bauwe H, Kaplan A, Hagemann M (2006) The plant-like C2 glycolate cycle and the bacterial-like glycerate pathway cooperate in phosphoglycolate metabolism in cyanobacteria. Plant Physiol **142:** 333–342

Eisenhut M, Ruth W, Haimovich M, Bauwe H, Kaplan A, Hagemann M (2008) The photorespiratory glycolate metabolism is essential for cyanobacteria and might have been conveyed endosymbiontically to plants. Proc Natl Acad Sci USA **105:** 17199–17204

Ermakova M, Battchikova N, Richaud P, Leino H, Kosourov S, Isojärvi J, Peltier G, Flores E, Cournac L, Allahverdiyeva Y, et al (2014) Heterocyst-specific flavodiiron protein Flv3B enables oxic diazotrophic growth of the filamentous cyanobacterium Anabaena sp. PCC 7120. Proc Natl Acad Sci USA **111:** 11205–11210

Feilke K, Yu Q, Beyer P, Sétif P, Krieger-Liszkay A (2014) In vitro analysis of the plastid terminal oxidase in photosynthetic electron transport. Biochim Biophys Acta **1837:** 1684–1690

Graan T, Ort DJ (1986) Detection of oxygen-evolving photosystem II centers inactive in plastoquinone reduction. Biochim Biophys Acta **852:** 320–330

Hart SE, Schlarb-Ridley BG, Bendall DS, Howe CJ (2005) Terminal oxidases of cyanobacteria. Biochem Soc Trans **33:** 832–835

Helman Y, Barkan E, Eisenstadt D, Luz B, Kaplan A (2005) Fractionation of the three stable oxygen isotopes by oxygen-producing and oxygen-consuming reactions in photosynthetic organisms. Plant Physiol **138:** 2292–2298

Helman Y, Tchernov D, Reinhold L, Shibata M, Ogawa T, Schwarz R, Ohad I, Kaplan A (2003) Genes encoding A-type flavoproteins are essential for photoreduction of O_2 in cyanobacteria. Curr Biol **13:** 230–235

Heyno E, Gross CM, Laureau C, Culcasi M, Pietri S, Krieger-Liszkay A (2009) Plastid alternative oxidase (PTOX) promotes oxidative stress when overexpressed in tobacco. J Biol Chem **284:** 31174–31180

Hihara Y, Sonoike K, Kanehisa M, Ikeuchi M (2003) DNA microarray analysis of redox-responsive genes in the genome of the cyanobacterium Synechocystis sp. strain PCC 6803. J Bacteriol **185:** 1719–1725

Howitt CA, Cooley JW, Wiskich JT, Vermaas WF (2001) A strain of Synechocystis sp. PCC 6803 without photosynthetic oxygen evolution and respiratory oxygen consumption: implications for the study of cyclic photosynthetic electron transport. Planta **214:** 46–56

Howitt CA, Udall PK, Vermaas WF (1999) Type 2 NADH dehydrogenases in the cyanobacterium Synechocystis sp. strain PCC 6803 are involved in regulation rather than respiration. J Bacteriol **181:** 3994–4003

Howitt CA, Vermaas WF (1998) Quinol and cytochrome oxidases in the cyanobacterium Synechocystis sp. PCC 6803. Biochemistry **37:** 17944–17951

Huang C, Yuan X, Zhao J, Bryant DA (2003) Kinetic analyses of state transitions of the cyanobacterium Synechococcus sp. PCC 7002 and its mutant strains impaired in electron transport. Biochim Biophys Acta **1607:** 121–130

Huang F, Parmryd I, Nilsson F, Persson AL, Pakrasi HB, Andersson B, Norling B (2002) Proteomics of Synechocystis sp. strain PCC 6803: identification of plasma membrane proteins. Mol Cell Proteomics **1:** 956–966

Iwata S, Ostermeier C, Ludwig B, Michel H (1995) Structure at 2.8 A resolution of cytochrome c oxidase from Paracoccus denitrificans. Nature **376:** 660–669

Joliot P, Johnson GN (2011) Regulation of cyclic and linear electron flow in higher plants. Proc Natl Acad Sci USA **108:** 13317–13322

Kok B (1949) On the interrelation of respiration and photosynthesis in green plants. Biochim Biophys Acta **3:** 625–631

Kranzler C, Lis H, Finkel OM, Schmetterer G, Shaked Y, Keren N (2014) Coordinated transporter activity shapes high-affinity iron acquisition in cyanobacteria. ISME J **8:** 409–417

Kufryk G, Vermaas W (2006) Sll1717 affects the redox state of the plastoquinone pool by modulating quinol oxidase activity in thylakoids. J Bacteriol **188:** 1286–1294

Lea-Smith DJ, Bombelli P, Vasudevan R, Howe CJ (2016) Photosynthetic, respiratory and extracellular electron transport pathways in cyanobacteria. Biochim Biophys Acta **1857:** 247–255

Lea-Smith DJ, Ross N, Zori M, Bendall DS, Dennis JS, Scott SA, Smith AG, Howe CJ (2013) Thylakoid terminal oxidases are essential for the cyanobacterium *Synechocystis* sp. PCC 6803 to survive rapidly changing light intensities. Plant Physiol **162:** 484–495

Liu LN, Bryan SJ, Huang F, Yu J, Nixon PJ, Rich PR, Mullineaux CW (2012) Control of electron transport routes through redox-regulated redistribution of respiratory complexes. Proc Natl Acad Sci USA **109:** 11431–11436

Matthijs HC, Lubberding HJ (1988) Dark respiration in cyanobacteria. *In* LJ Rogers, JR Gallon, eds, Biochemistry of the Algae and Cyanobacteria. Clarendon Press, Oxford, pp 131–145

McDonald AE, Ivanov AG, Bode R, Maxwell DP, Rodermel SR, Hüner NP (2011) Flexibility in photosynthetic electron transport: the physiological role of plastoquinol terminal oxidase (PTOX). Biochim Biophys Acta **1807:** 954–967

Mi H, Endo T, Schreiber U, Ogawa T, Asada K (1992) Electron donation from cyclic and respiratory flows to the photosynthetic intersystem chain is mediated by pyridine nucleotide dehydrogenase in the cyanobacterium Synechocystis PCC 6803. Plant Cell Physiol **33:** 1233–1237

Mullineaux CW (2014a) Co-existence of photosynthetic and respiratory activities in cyanobacterial thylakoid membranes. Biochim Biophys Acta **1837:** 503–511

Mullineaux CW (2014b) Electron transport and light-harvesting switches in cyanobacteria. Front Plant Sci **5:** 7

Mullineaux CW, Allen JF (1986) The state 2 transition in the cyanobacterium Synechococcus 6301 can be driven by respiratory electron flow into the plastoquinone pool. FEBS Lett **205:** 155–160

Mustila H, Paananen P, Battchikova N, Santana-Sanchez A, Muth-Pawlak D, Hagemann M, Aro EM, Allahverdiyeva Y (2016) The flavodiiron protein Flv3 functions as a homo-oligomer during stress acclimation and is distinct from the Flv1/Flv3 hetero-oligomer specific to the O2 photoreduction pathway. Plant Cell Physiol http://dx.doi.org/10.1093/pcp/pcw047

Nishio JN, Whitmarsh J (1993) Dissipation of the proton electrochemical potential in intact chlorophasts. II. The pH gradient monitored by cytochrome *f* reduction kinetics. Plant Physiol **101:** 89–96

Nomura CT, Persson S, Shen G, Inoue-Sakamoto K, Bryant DA (2006) Characterization of two cytochrome oxidase operons in the marine cyanobacterium Synechococcus sp. PCC 7002: inactivation of ctaDI affects the PS I:PS II ratio. Photosynth Res **87:** 215–228

Ohkawa H, Pakrasi HB, Ogawa T (2000) Two types of functionally distinct NAD(P)H dehydrogenases in Synechocystis sp. strain PCC6803. J Biol Chem **275:** 31630–31634

Pils D, Gregor W, Schmetterer G (1997) Evidence for in vivo activity of three distinct respiratory terminal oxidases in the cyanobacterium Synechocystis sp. strain PCC6803. FEMS Microbiol **152:** 83–88

Pils D, Schmetterer G (2001) Characterization of three bioenergetically active respiratory terminal oxidases in the cyanobacterium Synechocystis sp. strain PCC 6803. FEMS Microbiol Lett **203:** 217–222

Pisareva T, Shumskaya M, Maddalo G, Ilag L, Norling B (2007) Proteomics of Synechocystis sp. PCC 6803: identification of novel integral plasma membrane proteins. FEBS J **274:** 791–804

Scherer S (1990) Do photosynthetic and respiratory electron transport chains share redox proteins? Trends Biochem Sci **15:** 458–462

Schneider D, Berry S, Rich P, Seidler A, Rögner M (2001) A regulatory role of the PetM subunit in a cyanobacterial cytochrome b6f complex. J Biol Chem **276:** 16780–16785

Schneider D, Berry S, Volkmer T, Seidler A, Rögner M (2004) PetC1 is the major Rieske iron-sulfur protein in the cytochrome b6f complex of Synechocystis sp. PCC 6803. J Biol Chem **279:** 39383–39388

Schultze M, Forberich B, Rexroth S, Dyczmons NG, Roegner M, Appel J (2009) Localization of cytochrome b6f complexes implies an incomplete respiratory chain in cytoplasmic membranes of the cyanobacterium Synechocystis sp. PCC 6803. Biochim Biophys Acta **1787:** 1479–1485

Schuurmans RM, Schuurmans JM, Bekker M, Kromkamp JC, Matthijs HCP, Hellingwerf KJ (2014) The redox potential of the plastoquinone pool of the cyanobacterium *Synechocystis* species strain PCC 6803 is under strict homeostatic control. Plant Physiol **165:** 463–475

Shen G, Boussiba S, Vermaas WFJ (1993) *Synechocystis* sp PCC 6803 strains lacking photosystem I and phycobilisome function. Plant Cell **5:** 1853–1863

Suorsa M, Grieco M, Järvi S, Gollan PJ, Kangasjärvi S, Tikkanen M, Aro EM (2013) PGR5 ensures photosynthetic control to safeguard photosystem I under fluctuating light conditions. Plant Signal Behav **8:** e22741

Tsunoyama Y, Bernát G, Dyczmons NG, Schneider D, Rögner M (2009) Multiple Rieske proteins enable short- and long-term light adaptation of Synechocystis sp. PCC 6803. J Biol Chem **284:** 27875–27883

Vass I, Kirilovsky D, Etienne AL (1999) UV-B radiation-induced donor- and acceptor-side modifications of photosystem II in the cyanobacterium Synechocystis sp. PCC 6803. Biochemistry **38:** 12786–12794

Vermaas W (2001) Photosynthesis and respiration in cyanobacteria. *In* eLS, John Wiley & Sons, London,

Vicente JB, Gomes CM, Wasserfallen A, Teixeira M (2002) Module fusion in an A-type flavoprotein from the cyanobacterium Synechocystis condenses a multiple-component pathway in a single polypeptide chain. Biochem Biophys Res Commun **294:** 82–87

Yan J, Kurisu G, Cramer WA (2006) Intraprotein transfer of the quinone analogue inhibitor 2,5-dibromo-3-methyl-6-isopropyl-p-benzoquinone in the cytochrome b_6f complex. Proc Natl Acad Sci USA **103:** 169–174

Yu Q, Feilke K, Krieger-Liszkay A, Beyer P (2014) Functional and molecular characterization of plastid terminal oxidase from rice (Oryza sativa). Biochim Biophys Acta **1837:** 1284–1292

Zhang L, Selão TT, Pisareva T, Qian J, Sze SK, Carlberg I, Norling B (2013) Deletion of Synechocystis sp. PCC 6803 leader peptidase LepB1 affects photosynthetic complexes and respiration. Mol Cell Proteomics **12:** 1192–1203

Zhang P, Allahverdiyeva Y, Eisenhut M, Aro EM (2009) Flavodiiron proteins in oxygenic photosynthetic organisms: photoprotection of photosystem II by Flv2 and Flv4 in Synechocystis sp. PCC 6803. PLoS ONE **4:** e5331